

Effect of a dynamic cooperative lane-changing algorithm on traffic evolution of connected and automated vehicles system at diverging on two-lane highways

Shuang Ren(任爽), Shuichao Zhang(张水潮), Huaqing Liu(刘华清), and Chen Zheng(郑晨)
Citation: Chin. Phys. B, 2026, 35 (**7**): 074702. DOI: 10.1088/1674-1056/ae27ae
http://cpb.iphy.ac.cn; http://iopscience.iop.org/cpb

What follows is a list of articles you may be interested in

Learning complex nonlinear physical systems using wavelet neural operators

Yanan Guo(郭亚楠), Xiaoqun Cao(曹小群), Hongze Leng(冷洪泽), and Junqiang Song(宋君强)
Chin. Phys. B, 2025, 34 (**3**): 034702. DOI: 10.1088/1674-1056/ada7dc

Shedding vortex simulation method based on viscous compensation technology research

Hao Zhou(周昊), Lei Wang(汪雷), Zhang-Feng Huang(黄章峰), and Jing-Zhi Ren(任晶志)
Chin. Phys. B, 2022, 31 (**4**): 044702. DOI: 10.1088/1674-1056/ac29ae

A new mixed subgrid-scale model for large eddy simulation of turbulent drag-reducing flows of viscoelastic fluids

Li Feng-Chen (李凤臣), Wang Lu (王璐), Cai Wei-Hua (蔡伟华)
Chin. Phys. B, 2015, 24 (**7**): 074701. DOI: 10.1088/1674-1056/24/7/074701

Effect of a dynamic cooperative lane-changing algorithm on traffic evolution of connected and automated vehicles system at diverging on two-lane highways

Shuang Ren(任爽)[1,2], Shuichao Zhang(张水潮)[1,2,†], Huaqing Liu(刘华清)[1,2,‡], and Chen Zheng(郑晨)[1,2]

[1] *School of Civil and Transportation Engineering, Ningbo University of Technology, Ningbo* 315211, *China*
[2] *Zhejiang Engineering Research Center of Digital Road Construction Technology, Hangzhou* 310012, *China*

(Received 16 September 2025; revised manuscript received 20 November 2025; accepted manuscript online 4 December 2025)

The diverging sections of two-lane highways are a typical traffic bottleneck in urban cities. Due to unregulated lane-changing (LC) behaviors, velocity oscillation and traffic congestion frequently occur. In this paper, a dynamic cooperative lane-changing (DCLC) algorithm is introduced to coordinate the LC behaviors of connected autonomous vehicles (CAVs) in a control zone upstream of the diverging point. For a CAV with LC demand, its virtual leader and follower on the adjacent lane are dynamically determined based on relative distances in real time. It will change lane if the safety time gap is satisfied. With the normal lane-changing algorithm as a benchmark, the phase transition and evolution of the traffic system are investigated and compared. Simulation results demonstrate that the proposed DCLC algorithm has a positive effect on traffic capacity. After the DCLC algorithm is implemented, the LC behaviors of CAVs are concentrated in the middle of the control zone, rather than being distributed near the diverging point in the benchmark. Moreover, some system characteristics have also been improved significantly. Finally, the sensitivities of demand and safety time gap in LC are analyzed to verify the universality of the DCLC algorithm in improving traffic performance.

Keywords: diverging, cooperative adaptive cruise control (CACC), virtual vehicles, lane-changing (LC), monetary cost

PACS: 47.27.E–, 47.27.T–, 45.70.Vn, 45.05.+x

DOI: 10.1088/1674-1056/ae27ae **CSTR:** 32038.14.CPB.ae27ae

1. Introduction

In the diverging of urban cities, lane-changing (LC) behaviors usually lead to some negative impacts on traffic flow, such as capacity drop,[1] collision risk,[2,3] and traffic oscillation.[4] Owing to the advancement of wireless communication, connected autonomous vehicles (CAVs) exhibit remarkable improvements in controllability and operational efficiency, which can improve traffic safety[5,6] and enhance traffic capacity.[7]

The longitudinal motion of vehicles is mainly reflected in car-following behavior, which will significantly influence the evolutionary characteristics of traffic systems. When the mechanical structure of vehicles remains unknown or undefined, some human-like models are used to model the longitudinal motion of CAVs, such as intelligent driver model (IDM)[8] and full velocity difference model (FVD).[9] If the mechanical structure can be predefined or modeled, the hierarchical control algorithm[10–12] is one of the widely used approaches. The upper-level control algorithm is pre-set to obtain the command acceleration[10,13] and the lower-level controller is constructed to model and simulate the mechanical transmission.[12,14,15] Among them, adaptive cruise control (ACC)[16,17] is a typical longitudinal car-following algorithm, designed based on feedback control using information collected by the onboard sensing equipment of the preceding vehicle. As an enhancement of ACC, cooperative adaptive cruise control (CACC)[11,18] is a systematic algorithm that improves traffic operation by connecting vehicles via vehicle-to-vehicle (V2V) or vehicle-to-infrastructure (V2I) communication.

The lateral motion of vehicles is mainly manifested as lane-changing (LC) behavior, usually including mandatory lane-changing (MLC) and discretionary lane-changing (DLC).[19] For CAVs with LC demand, lateral control algorithms are designed to coordinate LC behaviors with other vehicles on adjacent lanes, such as the gap-based approach,[20,21] the minimizing overall braking induced by lane changes (MOBIL) approach,[22,23] and the game theory-based approach.[24,25] When the ego vehicle is performing LC behavior, its safety is usually ensured. The lateral motion does not significantly affect vehicles' longitudinal car-following. Thus, in some investigations[22,26,27] LC can be simplified to instantaneous behavior. When the research focuses on the game between lane-changing vehicles and the surrounding vehicles, it is necessary to establish a correlation model between deceleration and lateral movement. Meanwhile, instantaneous LC is no longer applicable.[28,29]

†Corresponding author. E-mail: zhangshuichao@nbut.edu.cn
‡Corresponding author. E-mail: liuhuaqing@nbut.edu.cn

© 2026 Chinese Physical Society and IOP Publishing Ltd. All rights, including for text and data mining, AI training, and similar technologies, are reserved.

Numerous studies have demonstrated that appropriate cooperative strategies at merging are implemented for CAVs in a control zone and can significantly improve traffic efficiency.[30–32] One approach is heuristic rule-based algorithm,[33–35] such as virtual vehicles[33,34] and virtual platoon[35] by mapping a single vehicle or a platoon of CAVs onto an adjacent lane. The second approach is an optimization-based control algorithm,[28,32,36] such as mixed integer programming[28,32] and model predictive control.[36] The third approach is a machine learning-based control algorithm, such as neural networks[37] and machine learning methods.[38] In comparison, heuristic rule-based algorithms exhibit both higher computational efficiency and a distinct advantage in real-time implementation.

However, studies on cooperative lane-changing algorithms and how traffic flow evolves at diverging areas are still limited. Motivated by this fact, in this paper, a dynamic cooperative lane-changing (DCLC) algorithm is designed for CAVs to coordinate LC behaviors at diverging areas. For a CAV with LC demand in the control zone, its target preceding and following vehicles on the adjacent lane are detected in real time. Virtual vehicles are applied to determine the sequence of car-following, and a virtual chain is updated dynamically according to the relative location. Under the proposed DCLC algorithm, traffic evolution is systematically discussed and compared with a benchmark.

The rest of the paper is organized as follows. In Section 2, the longitudinal control algorithm of CAVs and the DCLC algorithm are proposed. In Section 3, simulations of traffic evolution under the proposed DCLC algorithm and benchmark are performed and compared. Finally, Section 4 gives the conclusions.

2. The control algorithm

2.1. Traffic scenario and assumptions

Figure 1 shows the geometric layout of a typical diverging bottleneck on two-lane highways. The control zone is located upstream of the diverging point. The LC behaviors of CAVs are assumed to be concentrated in the control zone for improving traffic efficiency. Furthermore, delay and packet loss in communication are not taken into account.[8,9,21,22]

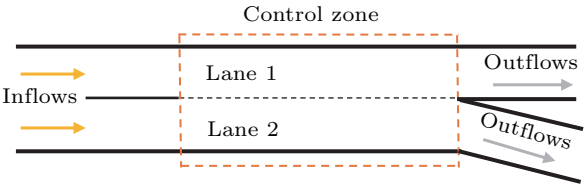


Fig. 1. The geometric layout.

2.2. Control algorithm outside control zone

The hierarchical control algorithm containing the upper-level control algorithm and the lower-level controller is used to model the longitudinal car-following of CAVs in this paper, as follows:

$$\text{Upper-level:}\quad a_{\text{cmd}} = k_{\text{a}}a_{\text{p}} + k_{\text{v}}\left(v_{\text{p}} - v_{\text{ego}}\right) + k_{\text{g}}\left(g_{\text{ego}} - g_{\text{desire}}\right), \tag{1}$$

$$\text{Lower-level:}\quad a + \tau\dot{a} = a_{\text{cmd}}. \tag{2}$$

In Eq. (1), the command acceleration a_{cmd} is calculated with the acceleration a_{p}, velocity difference $v_{\text{p}} - v_{\text{ego}}$ and the difference between actual spacing g_{ego} and desired spacing g_{desire}.

$$g_{\text{ego}} = x_{\text{p}} - x_{\text{ego}}, \tag{3}$$

$$g_{\text{desire}} = L_{\text{c}} + G_{\text{min}} + T_{\text{g}}v_{\text{ego}}. \tag{4}$$

$[a_{\text{p}}, v_{\text{p}}, x_{\text{p}}]$ denotes the acceleration, velocity and location of the preceding vehicle in the same lane. $[v_{\text{ego}}, x_{\text{ego}}]$ denotes the velocity and location of the ego vehicle. The desired spacing g_{desire} is determined by the constant time headway policy with time gap T_{g}. L_{c} and G_{min} denote the length of the vehicle and the standstill distance. The gain parameters k_{a}, k_{v} and k_{g} denote the control gains. In Eq. (2), the first-order lag model with average response time τ is used to approximate the mechanical transmission.

2.3. DCLC in control zone

2.3.1. Dynamic cooperative algorithm

Figure 2 depicts the schematic diagram of the proposed dynamic cooperative algorithm using virtual vehicles in the control zone. Virtual vehicles are introduced by mapping vehicles from an adjacent lane onto the current lane. For the ego vehicle numbered D with LC demand, the virtual sequence chain C-D-E, containing its target preceding and following vehicles on the adjacent lane, is formed in real time and dynamically updated at each time step. If vehicle D overtakes its virtual leading vehicle C, a new virtual sequence chain A-D-C is generated and then it is converted into a virtual predecessor–follower relationship with vehicle C, as shown in Fig. 2(b). After vehicle D completes LC, the virtual sequence chain is no longer triggered, and it resumes following its preceding vehicle on the ego lane.

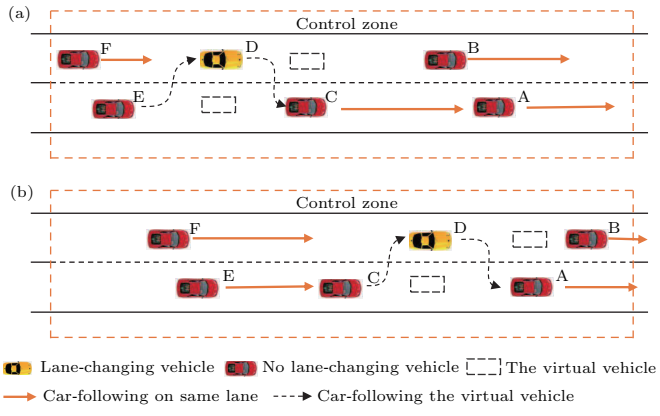


Fig. 2. An updated example of virtual sequence chain.

CAVs perform car-following in accordance with the virtual sequence chain. If the ego vehicle follows its virtual preceding vehicle, the command acceleration denoted as $a_{\mathrm{cmd,virtual}}$ is calculated as follows:

$$a_{\mathrm{cmd,virtual}} = \min\left(k_{\mathrm{a}}a_{\mathrm{p,virtual}} + k_{\mathrm{v}}\left(v_{\mathrm{p,virtual}} - v_{\mathrm{ego}}\right) + k_{\mathrm{g}}\left(g_{\mathrm{virtual}} - g_{\mathrm{desire}}\right), a_{\mathrm{cmd,lim}}\right), \tag{5}$$

in which $a_{\mathrm{cmd,lim}}$ denotes the limitation on deceleration. The command acceleration following the preceding vehicle on the ego lane, denoted as $a_{\mathrm{cmd,ego}}$, is obtained by

$$a_{\mathrm{cmd,ego}} = k_{\mathrm{a}}a_{\mathrm{p,ego}} + k_{\mathrm{v}}\left(v_{\mathrm{p,ego}} - v_{\mathrm{ego}}\right) + k_{\mathrm{g}}\left(g_{\mathrm{ego}} - g_{\mathrm{desire}}\right). \tag{6}$$

To avoid the risk of collisions on the same lane due to insufficient deceleration, the actual command acceleration is determined by

$$a_{\mathrm{cmd}} = \min\left(a_{\mathrm{cmd,virtual}}, a_{\mathrm{cmd,ego}}\right). \tag{7}$$

Moreover, some physical constraints are introduced as follows:

$$v_{\min} \le v \le v_{\max}, \tag{8}$$

$$a_{\min} \le a_{\mathrm{cmd}} \le a_{\max}, \tag{9}$$

$$J_{\min} \le \dot{a} \le J_{\max}. \tag{10}$$

Table 1 exhibits the values of parameters used in the simulation. In Ref. [33], our previous study proved the stability region with gain parameters k_{a}, k_{v}, and k_{g}. Moreover, the minimum gap and velocity of the following CAV are negatively correlated with k_{g} when the preceding CAV decelerates at $J_{\min}$ until its acceleration reaches $a_{\min}$. A small k_{g} contributes to enhancing safety in car-following when the preceding vehicle undergoes extreme deceleration.

Table 1. The value of parameters in the simulation.

Parameter	Value	Parameter	Value
$v_{\max}$	30 m/s	k_{a}	0.3
$v_{\min}$	0 m/s	k_{v}	1.5 s^{-1}
$a_{\max}$	3 $\mathrm{m/s}^2$	k_{g}	0.1 s^{-2}
$a_{\min}$	−3 $\mathrm{m/s}^2$	τ	0.4 s
$J_{\max}$	2 $\mathrm{m/s}^3$	$G_{\min}$	2 m
$J_{\min}$	−2 $\mathrm{m/s}^3$	T_{g}	1.2 s
ΔT	0.1 s	T_{safe}	1.1 s
L_{c}	5 m		

2.3.2. LC strategy

When CAVs enter the control zone, the proposed dynamic cooperative algorithm is triggered and the adjustment of spacing is initiated to ensure smooth implementation of LC. When the time gaps between the ego vehicle and its target preceding/following vehicles simultaneously approach the safety time gap T_{safe}, it will immediately change lane, as shown in Fig. 3. The LC strategy is shown as follows:

$$\min\left[\left(x_{\mathrm{p,tar}} - x_{\mathrm{ego}} - L_{\mathrm{c}} - G_{\min}\right)/v_{\mathrm{ego}}, \left(\left(x_{\mathrm{ego}} - x_{\mathrm{f,tar}} - L_{\mathrm{c}} - G_{\min}\right)/v_{\mathrm{f,tar}}\right)\right] \ge T_{\mathrm{safe}}. \tag{11}$$

Notably, as the inflow rate and LC demand increase, traffic scenarios in which multiple consecutive CAVs need to change lanes will occur frequently. Figure 4 demonstrates schematic diagrams when two and three consecutive CAVs change lanes (when the number of consecutive vehicles increases further, the LC behavior follows a similar pattern). It is notable that the virtual sequence chain is detected and updated in real time at each time step. When the relative positions with respect to other vehicles with LC demand change, the virtual sequence chain is adjusted accordingly, which may even evolve into the traffic scenario shown in Fig. 3.

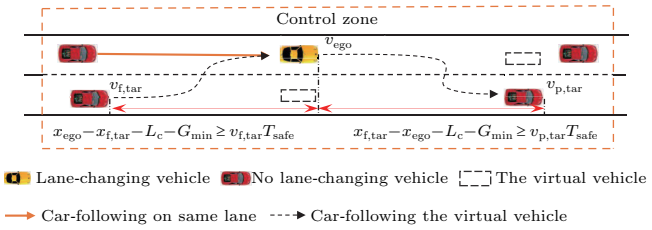


Fig. 3. LC strategy when one CAV changes lane.

When vehicles on different lanes perform car-following with the virtual sequence chain, as shown in Figs. 4(a) and 4(b), the time gaps between consecutive vehicles gradually change over time. Once the LC strategy is satisfied, one vehicle initiates lane-changing and its virtual vehicle is no longer maintained. The car-following and LC behaviors of other vehicles in the established original virtual sequence chain are not affected. For example, after vehicle C changes lanes, the distance between vehicle D and the preceding vehicle on the target lane changes from C to A and becomes larger, as shown in Fig. 4(a).

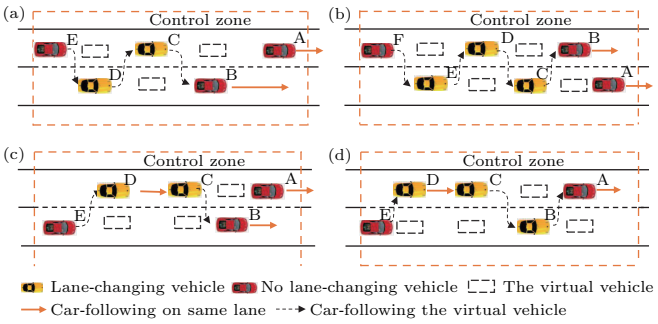


Fig. 4. LC strategy when consecutive multi CAVs change lanes.

When two consecutive vehicles (vehicles C and D) in the virtual sequence chain are located on the same lane, as shown

in Figs. 4(c) and 4(d), the preceding/following vehicle on the ego lane changes to the adjacent lane and its virtual vehicle is formed. Although the target vehicle in the LC strategy has changed, the time gap of the ego vehicle remains safe because the car-following sequence does not change. For example, after vehicle C changes lanes, the car-following sequence remains B–C–D–E (Fig. 4(c)) and A–B–C–D–E (Fig. 4(d)).

2.4. Benchmark

To evaluate the traffic efficiency under the DCLC algorithm, a normal LC algorithm is introduced as a benchmark. The control zone is replaced with a free LC zone and a mandatory LC zone, as shown in Fig. 5. Without cooperation with nearby vehicles on the adjacent lane, the ego vehicle maintains car-following of its preceding vehicle in the free LC zone. The ego vehicle also performs real-time detection to check whether Eq. (11) is satisfied. When it enters the mandatory LC zone, yielding behavior of its target following vehicle on the adjacent lane is introduced. (Yielding behavior means that in the mandatory LC zone, the ego vehicle follows the nearest preceding vehicle on the adjacent lane based on Eqs. (5)–(7) and $a_{\mathrm{cmd,lim}} = -\infty$ m/s^2. Under an oversaturated inflow rate, the velocity is low. The LC strategy in Eq. (11) becomes overly strict, which may cause vehicles to remain unable to initiate LC behavior until they stop at the diverging point side by side.) Note that yielding behavior of the following vehicle occurs only when (1) the following vehicle does not have LC demand but the gap to its preceding vehicle satisfies $x_{\mathrm{ego}} - x_{\mathrm{f,tar}} \geq \frac{T_{\mathrm{g}}}{2} v(t) + G_{\min}$, as shown in Figs. 5(a) and 5(b), or (2) the following vehicle has LC demand, as shown in Fig. 5(c) and 5(d). Moreover, collision prevention is also taken into account at each time step in the control zone, which is given as follows:

$$x_{\mathrm{p,tar}} - x_{\mathrm{ego}} - L_{\mathrm{c}} > s_{\mathrm{ego}}\big|_0^{T_{\mathrm{ego}}} - s_{\mathrm{p,tar}}\big|_0^{T_{\mathrm{p,tar}}}, \tag{12}$$

$$x_{\mathrm{ego}} - x_{\mathrm{f,tar}} - L_{\mathrm{c}} > s_{\mathrm{f,tar}}\big|_0^{T_{\mathrm{f,tar}}} - s_{\mathrm{ego}}\big|_0^{T_{\mathrm{ego}}}, \tag{13}$$

where $T_{\mathrm{p,tar}}$, $T_{\mathrm{f,tar}}$, and T_{ego} denote the time steps when the corresponding CAVs come to a complete stop. $s_{\mathrm{p,tar}}$ denotes the distance of the target preceding vehicle decelerating at $J_{\min}$ until it stops. s_{ego} and $s_{\mathrm{f,tar}}$ denote the distances of the two vehicles following their preceding vehicles based on Eqs. (3) and (4) from the current step to the stopping step. In particular, if the target following vehicle has not entered the mandatory LC zone, the safety LC time gap remains T_{safe}.

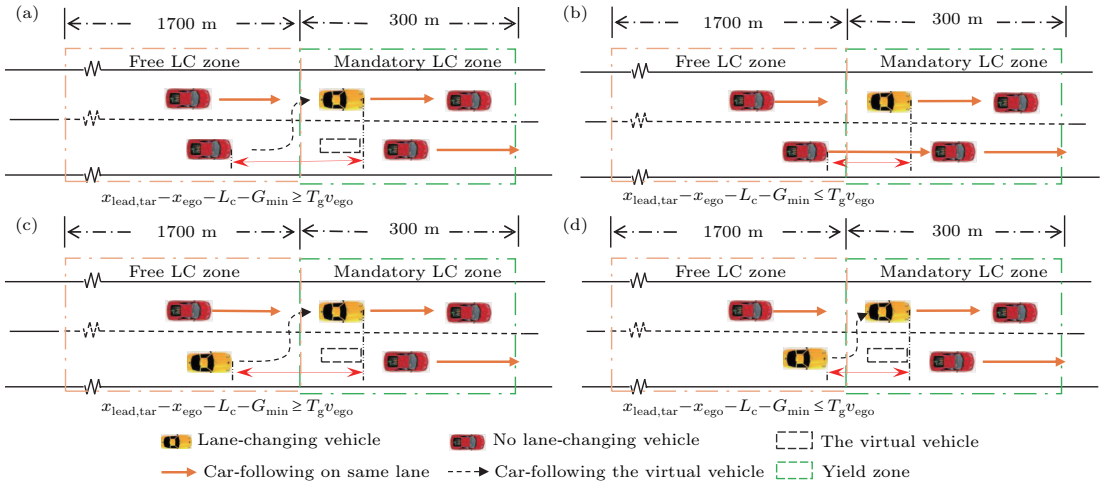


Fig. 5. Free LC zone and mandatory LC zone.

3. Simulation

In the simulation (30 runs were carried out for each entering probability P_{in}, and each simulation lasted 2000 s), the length l of the road section and the location of the diverging point are set to $x = 9000$ m and $x = 8000$ m, respectively. The control zone extends from $x = 6000$ m to $x = 8000$ m. Each new CAV enters the road section with probability P_{in} and the maximum velocity $v_{\max}$ if the last vehicle on the same lane is beyond $L_{\mathrm{c}} + G_{\min} + T_{\mathrm{g}} v_{\max}$. The proportions of vehicles with LC demand on Lanes 1 and 2 are denoted as $p_1 = 0.1$ and $p_2 = 0.3$, respectively. When the preceding vehicle on the same lane reaches the exit after the diverging point, it is removed, and the ego vehicle consequently follows a hypothetical vehicle at infinity.

3.1. Capacity

Figure 6 exhibits the dependence of flow rates on the entering probability P_{in}. It is noted that under both the proposed cooperative algorithm and the benchmark, there exists a threshold $P_{\mathrm{in}} = P_{\mathrm{c}}$. When $P_{\mathrm{in}} < P_{\mathrm{c}} \approx 0.23$, the traffic flow is free and the outflow is equal to the inflow. When $P_{\mathrm{in}} > P_{\mathrm{c}} \approx 0.23$, congestion forms and the total outflow $Q_{\mathrm{out}} = Q_{\mathrm{out},1} + Q_{\mathrm{out},2}$ remains constant. No capacity drop is observed. Under the benchmark, the traffic outflow and

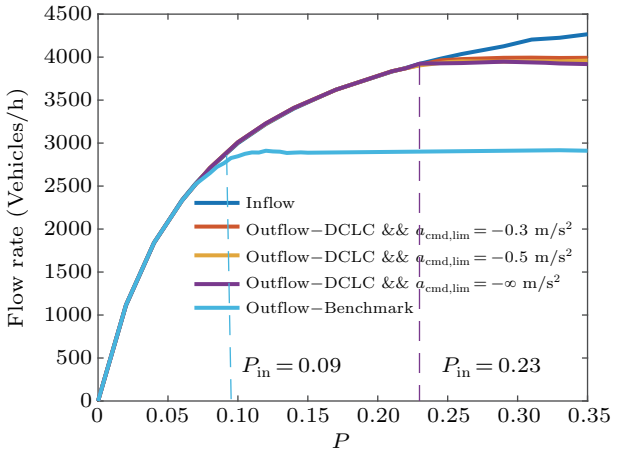


Fig. 6. The dependence of flow rates on entering probability P_{in}.

threshold P_{c} are 2835 vehicles/h and 0.09, respectively, which are significantly smaller than those under the DCLC algorithm. Note that the observed outflows for $a_{\mathrm{cmd,lim}} = -\infty$ m/s^2 and $a_{\mathrm{cmd,lim}} = -0.3$ m/s^2 are 3929 and 3992 vehicles/h, respectively, demonstrating an increase of 1.60%. Note that a small $|a_{\mathrm{cmd,lim}}|$ smooths the deceleration of CAVs and increases the average velocity after LC, thereby slightly increasing the outflow.

3.2. Spatiotemporal pattern

3.2.1. Spatiotemporal pattern of velocity

Figure 7 exhibits the comparison of the velocity spatiotemporal patterns at two typical inflow rates. When the

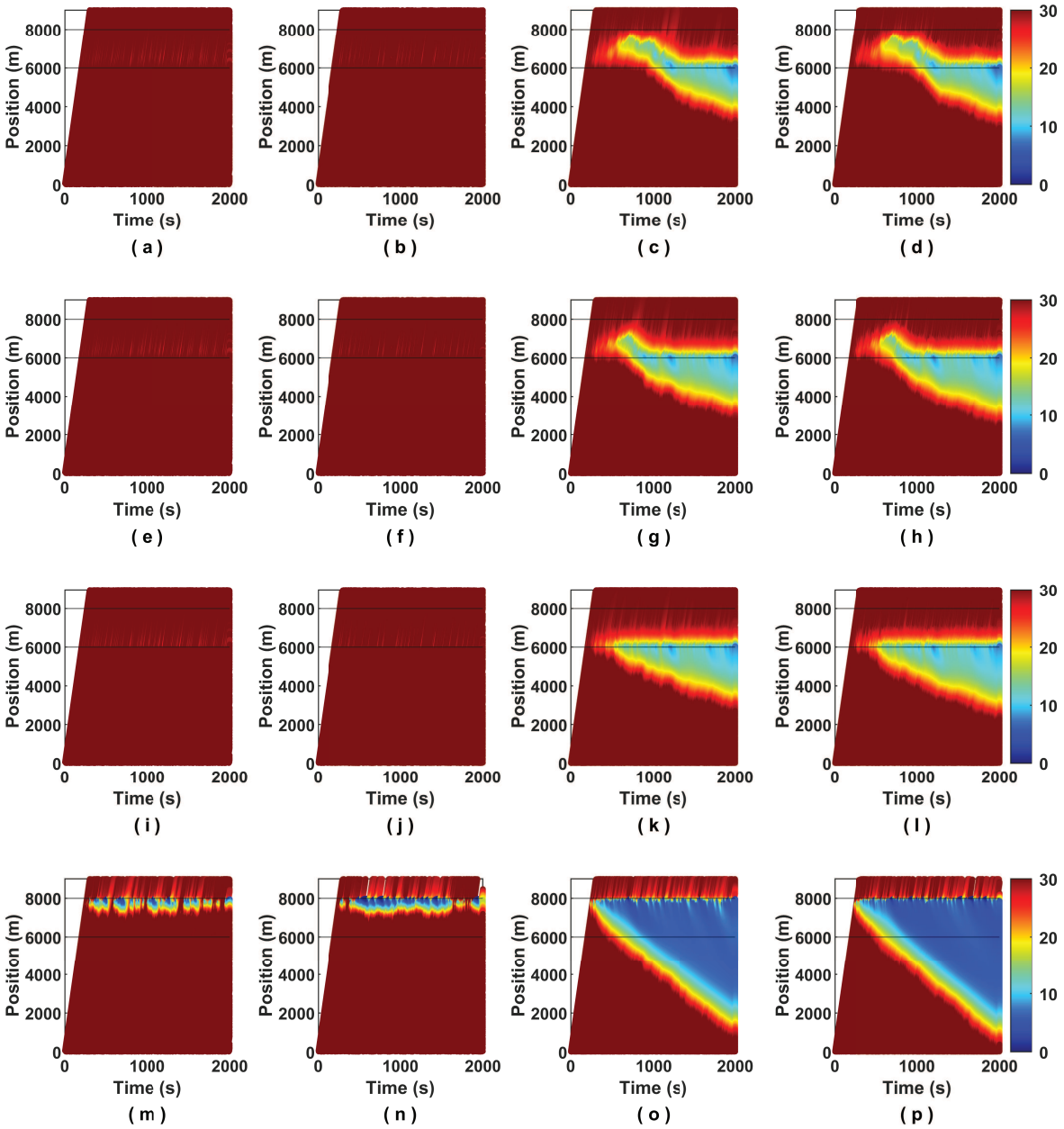


Fig. 7. Spatiotemporal pattern of speed (unit: m/s). (a)–(d): $a_{\mathrm{cmd,lim}} = -0.3$ m/s^2. (e)–(h) $a_{\mathrm{cmd,lim}} = -0.5$ m/s^2. (i)–(l) $a_{\mathrm{cmd,lim}} = -\infty$ m/s^2. (m)–(p) Benchmark. Columns 1 and 3: Lane 1; Columns 2 and 4: Lane 2; Columns 1 and 2: $P_{\mathrm{in}} = 0.07$; Columns 3 and 4: $P_{\mathrm{in}} = 0.33$.

inflow is undersaturated under the DCLC algorithm at $P_{\text{in}} = 0.07$ (seen in Figs. 7(a), 7(b), 7(e), 7(f), 7(i), and 7(j)), no congestion occurs. Moreover, the velocity spatiotemporal pattern is independent of $a_{\text{cmd,lim}}$. Nevertheless, some local congestion occurs under the benchmark, as shown in Figs. 7(m) and 7(n). When the inflow is oversaturated at $P_{\text{in}} = 0.33$ (seen in columns 3 and 4 of Fig. 7), traffic congestion forms and propagates upstream under both algorithms. Note that when $|a_{\text{cmd,lim}}| \leq 0.5$ m/s^2 under the DCLC algorithm in Figs. 7(c)–7(d) and 7(g)–7(h), a "two-stage" phase transition appears in the control zone, which is consistent with Ref. [33]. Affected by a small $|a_{\text{cmd,lim}}|$, CAVs perform smooth and coordinated cooperation with each other, and local congestion is formed. As P_{in} increases, congestion propagates upstream and forms a shock wave near the entrance of the control zone. Compared with the benchmark, congestion forms near the exit of the control zone and propagates upstream as a shock wave with a lower speed. It is noted that the speed of the shock wave on Lane 2 is faster than that on Lane 1 due to different LC demands on the two lanes. Under the DCLC algorithm, CAVs on both lanes are subjected to the same level of deceleration influence as a result of the virtual sequence chain. Consequently, there is no notable disparity in the spatiotemporal patterns between the two lanes.

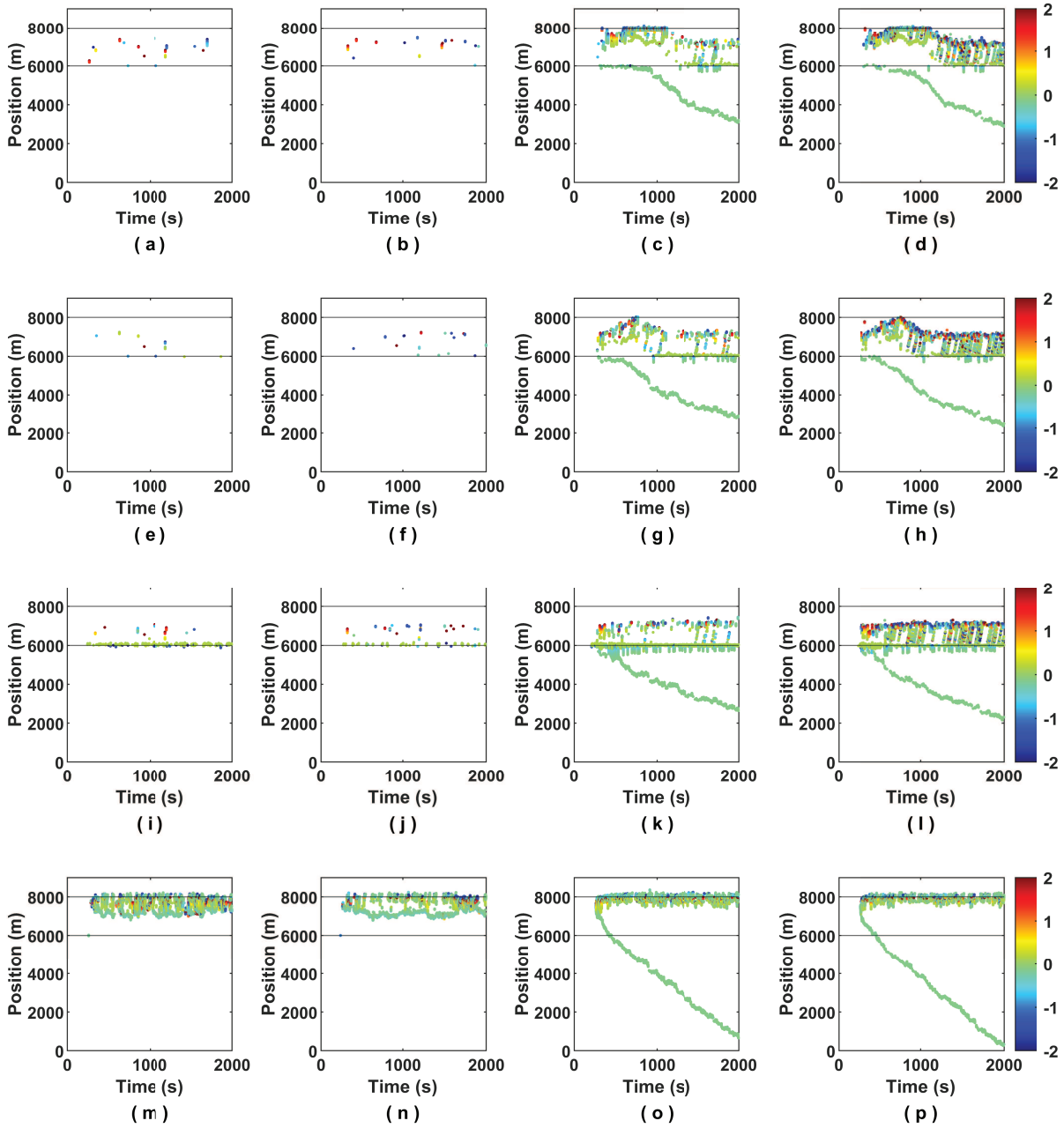


Fig. 8. Spatiotemporal pattern of notable jerk ($|J| > 0.1$) (unit: m/s^3). (a)–(d): $a_{\text{cmd,lim}} = -0.3$ m/s^2. (e)–(h): $a_{\text{cmd,lim}} = -0.5$ m/s^2. (i)–(l): $a_{\text{cmd,lim}} = -\infty$ m/s^2. (m)–(p): Benchmark. Columns 1 and 3: Lane 1; Columns 2 and 4: Lane 2; Columns 1 and 2: $P_{\text{in}} = 0.07$; Columns 3 and 4: $P_{\text{in}} = 0.33$.

3.2.2. Spatiotemporal pattern of jerk

Figure 8 depicts the spatiotemporal pattern of notable jerks ($|J| > 0.1$ m/s^3) under both undersaturated and oversaturated inflow conditions. It can be seen that in Figs. 8(a), 8(b), 8(e), 8(f), 8(i), and 8(j) at $P_{\text{in}} = 0.07$, a small number of notable jerks are sparsely distributed in the control zone under the DCLC algorithm. However, under the benchmark, a substantial number of notable jerks are scattered upstream of the exit of the control zone. When the inflow is oversaturated at $P_{\text{in}} = 0.33$ (seen in columns 3 and 4 of Fig. 8), notable jerks also occur at the fronts separating different traffic states.

3.2.3. The positions of LC

The control zone is discretized into cells of 10 m, and the frequency of LC in each cell is calculated, as shown in Table 1. Under the DCLC algorithm, the distribution of LC positions is influenced by $a_{\text{cmd,lim}}$ and exhibits a skewed distribution. When the inflow is undersaturated at $P_{\text{in}} = 0.07$, the LC strategy is easily satisfied and CAVs change lanes immediately upon entering the control zone. Hence, there exists a relatively high proportion of LC behaviors near the entrance of the control zone, as shown in Figs. 9(a) and 9(c). As P_{in} increases to an oversaturated inflow, as shown in Figs. 9(b) and 9(d), the DCLC algorithm is triggered and the gap between CAVs gradually expands. LC behaviors are mainly concentrated near the midpoint of the control zone. Under the benchmark, CAVs change lanes in the MLC zone. Furthermore, a smaller $|a_{\text{cmd,lim}}|$ leads to later lane-changing behavior.

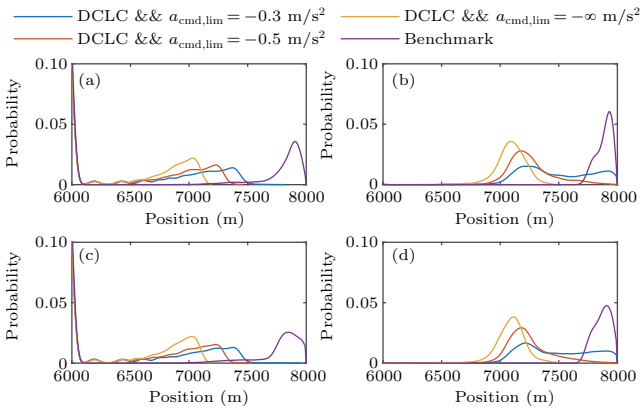


Fig. 9. Distribution of vehicle LC positions. Upper (a) and (b): Lane 1; Lower (c) and (d): Lane 2. Left (a) and (c): $P_{\text{in}} = 0.07$; Right (b) and (d): $P_{\text{in}} = 0.33$.

3.3. Safety

Time to collision (TTC) is widely used to quantify the safety performance of traffic systems.[39] Equation (14) represents the calculation of TTC between vehicle i and its leading vehicle $i-1$ on the same lane. It is noted that $\text{TTC}_i(t)$ is infinite at $v_i(t) = v_{i-1}(t)$. Thus, $\frac{1}{\text{TTC}_i(t)}$ is employed to evaluate the safety of vehicle i at time step t

$$\text{TTC}_i(t) = \begin{cases} \dfrac{x_{i-1}(t) - x_i(t) - L_{\text{c}}}{v_i(t) - v_{i-1}(t)}, & \text{if } v_i(t) > v_{i-1}(t), \\ \infty, & \text{if } v_i(t) \le v_{i-1}(t), \end{cases} \tag{14}$$

$$\text{MTTC}_i = \frac{1}{N}\sum_1^N \frac{1}{(t_{\text{out}} - t_{\text{in}})\Delta T} \sum_{t_{\text{in}}}^{t_{\text{out}}} \frac{1}{\text{TTC}_i(t)}, \tag{15}$$

where MTTC_i denotes the average $1/\text{TTC}$ of vehicle i passing through the control zone in N simulations. t_{in} and t_{out} are the entering and exiting time steps of the vehicle, respectively. Figure 10 demonstrates the dependence of MTTC on vehicle number at $P_{\text{in}} = 0.07$ and $P_{\text{in}} = 0.33$. It can be seen that the collision risk under the DCLC algorithm is much smaller than that under the benchmark. When the inflow is undersaturated at $P_{\text{in}} = 0.07$ in Figs. 10(a) and 10(c), MTTC nearly approaches a constant under the DCLC algorithm. When the inflow is oversaturated at $P_{\text{in}} = 0.33$ in Figs. 10(b) and 10(d), MTTC first increases due to the small gap caused by the oversaturated inflow and then remains constant under steady congestion.

A small $|a_{\text{cmd,lim}}|$ helps to suppress the aggravation of velocity differences and enhances safety to a certain extent. Under the benchmark, due to the higher LC demand on Lane 2 ($p_2 > p_1$), there appears a situation in the mandatory LC zone where $x_{i-1}(t) - x_i(t) - L_{\text{c}}$ is slightly larger than 0, which implies an extremely high $1/\text{TTC}$ and collision risk. Hence, this leads to some large peaks under the benchmark in Fig. 10.

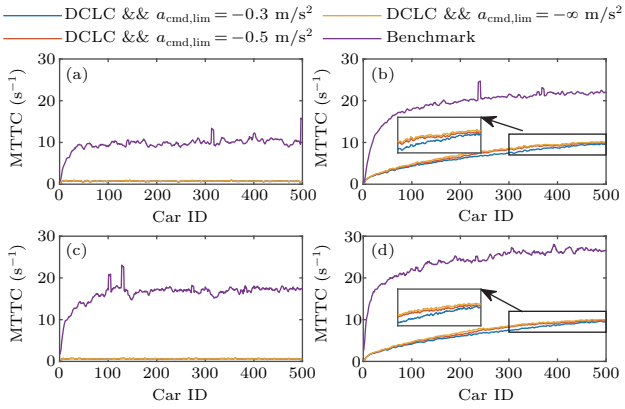


Fig. 10. Distribution of vehicle LC positions. Upper (a) and (b): Lane 1; Lower (c) and (d): Lane 2. Left (a) and (c): $P_{\text{in}} = 0.07$; Right (b) and (d): $P_{\text{in}} = 0.33$.

3.4. Fuel consumption

The discrete form of the proposed model in Ref. [40] is used to measure the fuel consumption of CAVs as follows:

$$E(\dot{x}_l(t), \ddot{x}_l(t)) = \sum_{t_{\text{in}}}^{t_{\text{out}}} \exp\left(\sum_{i=0}^{3}\sum_{j=0}^{3} K_{ij} \left(\dot{x}_{l(t)}\right)^i \left(\ddot{x}_l(t)\right)^j \Delta T\right), \tag{16}$$

in which K_{ij} are constant coefficients listed in Table 2 for $a \ge 0$ and $a < 0$.

Table 2. Coefficients of fuel consumption for $a \geq 0$ and $a > 0$.

K_{ij}	$a(t)$ is positive				$a(t)$ is negative			
	$j=0$	$j=1$	$j=2$	$j=3$	$j=0$	$j=1$	$j=2$	$j=3$
$i=0$	−7.735	0.2295	−5.61E−3	9.773E−5	−7.735	−0.01799	−4.27E−3	1.8829E−4
$i=1$	0.02799	0.0068	−7.722E−4	8.38E−6	0.02804	7.72E−3	8.375E−4	3.387E−5
$i=2$	−2.228E−4	−4.402E−5	7.90E−7	8.17E−7	−2.199E−4	−5.219E−5	−7.44E−6	2.77E−7
$i=3$	1.09E−6	4.80E−8	3.27E−8	−7.79E−9	1.08E−6	2.47E−7	4.87E−8	3.79E−10

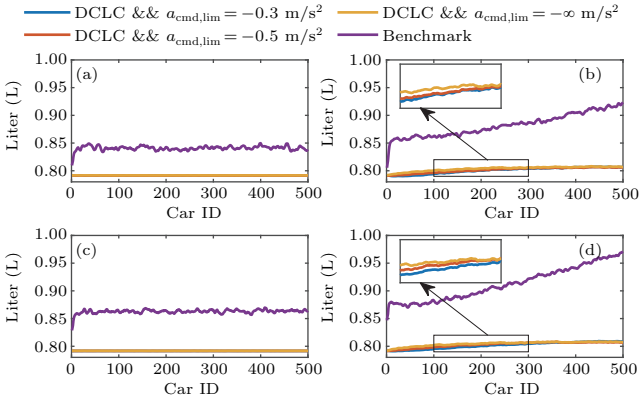


Fig. 11. Fuel consumption of each vehicle at two inflow rates. Upper (a) and (b): Lane 1; Lower (c) and (d): Lane 2. Left (a) and (c): $P_{in} = 0.07$; Right (b) and (d): $P_{in} = 0.33$.

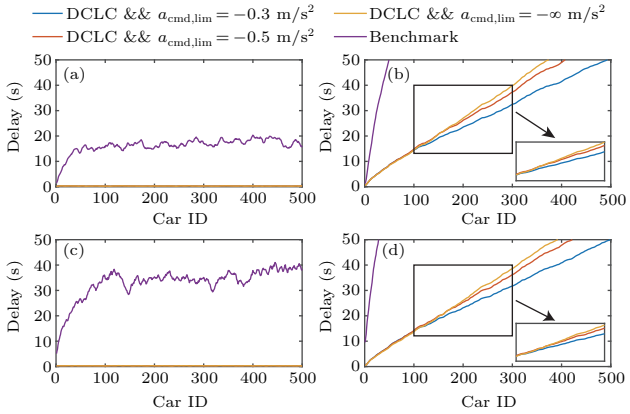


Fig. 12. Travel delay of each vehicle at two inflow rates. Upper (a) and (b): Lane 1; Lower (c) and (d): Lane 2. Left (a) and (c): $P_{in} = 0.07$; Right (b) and (d): $P_{in} = 0.33$.

Figure 11 shows the fuel consumption of vehicles under two algorithms. When the inflow is undersaturated, as shown in Figs. 11(a) and 11(c), the fuel consumption is independent of $a_{cmd,lim}$ and remains nearly constant, with values of 0.79 L under the DCLC algorithm and 0.84/0.86 L on Lane 1/2 under the benchmark. The improvement is about 6%/8%. When the inflow is oversaturated, as shown in Figs. 11(b) and 11(d), the fuel consumption first increases and then remains constant with vehicle number. Note that under the DCLC algorithm, a smaller $|a_{cmd,lim}|$ reduces the fuel consumption of vehicles entering earlier due to smoother deceleration. The effect of $|a_{cmd,lim}|$ on fuel consumption decreases progressively with the propagation of the shock wave outside the control zone. Compared with the benchmark, the proposed algorithm significantly reduces fuel consumption. Moreover, fuel consumption on Lane 2 is higher.

3.5. Travel delay

Travel delay is calculated as the difference between the total travel time and the minimum travel time. When the inflow is undersaturated in Figs. 12(a) and 12(c), travel delay is also independent of $a_{cmd,lim}$, which is 0.29 s under the DCLC algorithm and 16.32/33.23 s on Lane 1/2 under the benchmark. The improvement is about 98%/99%. When the inflow is oversaturated in Figs. 12(b) and 12(d), travel delay increases with vehicle number. Under the benchmark, travel delay exhibits a sharp linear increase with vehicle number. Compared with the benchmark, the travel delay under the DCLC algorithm is significantly reduced and is smallest at $a_{cmd,lim} = -0.3$ m/s^2.

3.6. Monetary costs

In order to comprehensively evaluate the performance of the proposed cooperative LC algorithm, the approach of monetary cost is applied in this paper. The cost-of-living data are obtained from NUMBEO (https://www.numbeo.com/cost-of-living/, May 10, 2025). The monthly salary and gasoline price are 6,743.95 ¥/month and 8.24 ¥/liter, respectively. The hourly wage (42.15 ¥/h) is calculated based on working 20 days a month and 8 hours a day.

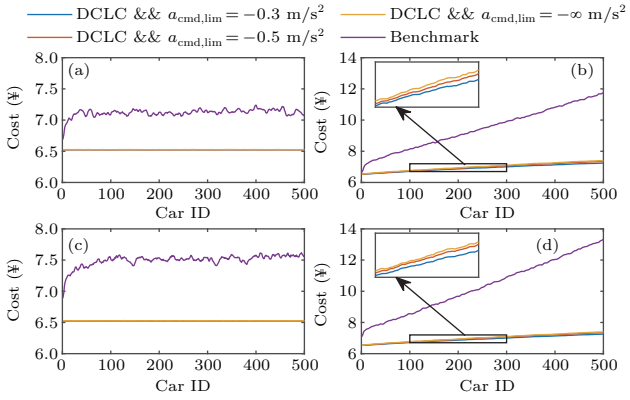


Fig. 13. Monetary cost via vehicle number at two typical inflows. Upper (a) and (b): Lane 1; Lower (c) and (d): Lane 2. Left (a) and (c): $P_{in} = 0.07$; Right (b) and (d): $P_{in} = 0.33$.

When the inflow is undersaturated in Figs. 13(a) and 13(c), under the benchmark the monetary costs of Lanes 1 and 2 are different and higher, which are ¥7.1 and ¥7.5, respectively. However, under the DCLC algorithm the monetary costs of CAVs are similar and approximately ¥6.52, with reductions of 8.2% and 13.1% on Lanes 1 and 2, respectively.

When the inflow is oversaturated in Figs. 13(b) and 13(d), the monetary costs increase with fuel consumption and travel delay. The superiority of the DCLC algorithm in reducing travel costs at diverging points can be clearly observed.

3.7. Sensitivity analysis

In this section, sensitivity analysis of the safe time gap T_{safe} and lane-changing demand on Lane 2 p_2 in the proposed DCLC algorithm ($a_{\text{cmd,lim}} = -\infty\ \text{m/s}^2$) and benchmark is performed and compared to verify the universality of the DCLC algorithm in improving traffic evolution. Table 3 compares the capacity under the two algorithms. One can see that the capacity increases with p_2 but decreases with T_{safe}. Moreover, the capacity under the DCLC algorithm is superior to that under the benchmark.

Table 3. The difference in capacity.

p_1:p_2	T_{safe}	Benchmark	DCLC
0.1:0.3	1.1	2835	3929(+38.59%)
	1.0	2885	4026(+39.55%)
	0.9	2963	4098(+38.31%)
0.1:0.2	1.1	2905	4211(+44.96%)
	1.0	2986	4327(+44.97%)
	0.9	3093	4434(+43.36%)
0.1:0.1	1.1	3063	4520(+47.57%)
	1.0	3090	4564(+47.70%)
	0.9	3180	4623(+45.38%)

Table 4. The differences in performance indicators under undersaturated inflow.

p_1:p_2	T_{safe}	Algorithm	Safety	Fuel consumption	Travel delay	Monetary cost
0.1:0.3	1.1	Benchmark	12.327	0.8517	23.285	7.2907
		DCLC	0.671(+94.56%)	0.7917(−7.04%)	0.284(−98.78%)	6.5271(−10.47%)
	1.0	Benchmark	11.090	0.8470	21.172	7.2272
		DCLC	0.638(+94.25%)	0.7918(−6.52%)	0.273(−98.71%)	6.5276(−9.68%)
	0.9	Benchmark	10.491	0.8439	19.686	7.1836
		DCLC	0.612(+94.17%)	0.7918(−6.17%)	0.264(−98.66%)	6.5279(−9.13%)
0.1:0.2	1.1	Benchmark	10.601	0.8446	20.699	7.2017
		DCLC	0.499(+95.29%)	0.7916(−6.28%)	0.196(−99.05%)	6.5253(−9.39%)
	1.0	Benchmark	8.801	0.8404	17.127	7.1256
		DCLC	0.477(+94.58%)	0.7917(−5.79%)	0.190(−98.89%)	6.5255(−8.42%)
	0.9	Benchmark	8.418	0.8356	15.851	7.071
		DCLC	0.458(+94.56%)	0.7917(−5.25%)	0.184(−98.84%)	6.5258(−7.71%)
0.1:0.1	1.1	Benchmark	8.834	0.8331	16.885	7.0623
		DCLC	0.344(+96.11%)	0.7915(−4.99%)	0.128(−99.24%)	6.5238(−7.62%)
	1.0	Benchmark	8.387	0.8303	16.643	7.0365
		DCLC	0.33(+96.07%)	0.7916(−4.66%)	0.124(−99.26%)	6.5239(−7.28%)
	0.9	Benchmark	7.368	0.8272	13.642	6.9754
		DCLC	0.319(+96.67%)	0.7916(−4.30%)	0.121(−99.12%)	6.5240(−6.48%)

Table 5. The differences in performance indicators under oversaturated inflow.

p_1:p_2	T_{safe}	Algorithm	Safety	Fuel consumption	Travel delay	Monetary cost
0.1:0.3	1.1	Benchmark	18.082	0.8700	113.446	8.496
		DCLC	5.494(+69.62%)	0.7980(−8.28%)	28.436(−74.93%)	6.908(−18.69%)
	1.0	Benchmark	17.734	0.8665	108.671	8.411
		DCLC	5.173(+70.83%)	0.8005(−7.62%)	23.788(−78.11%)	6.875(−18.27%)
	0.9	Benchmark	17.107	0.8632	103.081	8.319
		DCLC	4.872(+71.52%)	0.8015(−7.15%)	20.948(−79.68%)	6.850(−17.67%)
0.1:0.2	1.1	Benchmark	17.358	0.8637	105.172	8.348
		DCLC	3.931(+77.35%)	0.7935(−8.13%)	17.418(−83.44%)	6.742(−19.23%)
	1.0	Benchmark	16.616	0.8598	96.996	8.219
		DCLC	3.659(+77.98%)	0.7958(−7.62%)	13.817(−85.75%)	6.720(−18.25%)
	0.9	Benchmark	15.803	0.8562	89.244	8.099
		DCLC	3.403(+78.47%)	0.7969(−7.15%)	11.550(−87.06%)	6.702(−17.89%)
0.1:0.1	1.1	Benchmark	16.197	0.8536	93.356	8.126
		DCLC	2.342(+85.54%)	0.7909(−6.93%)	7.758(−91.69%)	6.608(−18.69%)
	1.0	Benchmark	15.614	0.8508	87.837	8.038
		DCLC	2.146(+86.26%)	0.7927(−6.83%)	5.792(−93.41%)	6.600(−17.89%)
	0.9	Benchmark	14.893	0.8485	81.514	7.945
		DCLC	1.967(+86.79%)	0.7936(−6.47%)	4.605(−94.35%)	6.593(−17.02%)

Tables 4 and 5 compare the differences in performance indicators under oversaturated and undersaturated inflows. The results are averaged over 20000 CAVs on both lanes across 50 runs. When the inflow is undersaturated in Table 4, compared with the benchmark, the improvements under the proposed DCLC algorithm are nearly 94.17%–96.67% in safety, 4.30%–7.04% in fuel consumption, 98.66%–99.26% in travel delay, and 6.48%–10.47% in monetary cost, respectively. When the inflow is oversaturated in Table 5, fuel consumption and monetary cost are further improved. Meanwhile, the safety of each vehicle increases with the reductions of p_2 and T_{safe}. Other performance indicators exhibit the opposite trend.

4. Conclusion

In this paper, a DCLC algorithm is proposed to coordinate the LC behaviors of CAVs at diverging. For a CAV with LC demand in the control zone, its target preceding and following vehicles on the neighboring lane are detected in real time, and a virtual sequence chain for cooperative car-following is updated at each time step. The normal lane-changing algorithm is considered as the benchmark.

In comparison with the benchmark, the simulations demonstrate that the DCLC algorithm can significantly improve the comprehensive performance of the CAV system at diverging sections on two-lane highways, particularly reflected in the substantial increase in total capacity on both lanes. Unlike the benchmark, the traffic evolution under the DCLC algorithm on both lanes is similar. Meanwhile, when $|a_{\text{cmd,lim}}| \leq 0.5\ \text{m/s}^2$ is under an oversaturated inflow in the DCLC algorithm, a "two-stage" phase transition appears in the control zone. Finally, sensitivity analysis of the LC demand on Lane 2 p_2 and safe time gap T_{safe} is conducted, which verifies the universality of the DCLC algorithm.

In future work, a cooperative algorithm based on virtual platooning will be developed to further investigate the impact of lane changing on system evolution.

Acknowledgments

This work was supported by the Natural Science Foundation of Zhejiang Province of China (Grant No. LTGG23E080005), the Scientific Research Project Funded by Ningbo University of Technology (Grant No. 2023KQ083), the General Research Project (Postgraduate Special) of Ningbo Institute of Technology (Grant No. 2024NGYA002), and research was supported by Ningbo Key Research and Development Plan Project (Grant No. 2023Z230)".

References

[1] Chen D J and Ahn S 2018 *Transp. Res. Part B Method.* **108** 1
[2] Qi H, Yao Y, Zhao X H, Guo J F, Zhang Y L and Bi C F 2022 *Physica A* **597** 127277
[3] Zhang J B, Lee J, Abdel-Aty M, Zheng O and Xiao G M 2023 *Accid. Anal. Prev.* **180** 106909
[4] Calvi A, Bella F and D'Amico F 2018 *J. Transp. Saf. Secur.* **10** 105
[5] Wang B, Luo Y G, Zhong Z H and Li K Q 2022 *Transp. Res. Part C Emerg. Technol.* **144** 103885
[6] Jiang Y S, Cong H W, Chen H Y and Yao Z H 2025 *Expert Syst. Appl.* **261** 125561
[7] Chen Y D, Kong D W, Sun L S, Zhang T and Song Y C 2022 *Physica A* **589** 126647
[8] Kim B and Heaslip K P 2023 *Int. J. Transp. Sci. Technol.* **12** 652
[9] Shen J, Zhao J D, Liu H Q, Jiang R and Yu Z X 2024 *Chin. Phys. B* **33** 030504
[10] Ruan T C, Chen Y J, Han G Y, Wang J, Li X P, Jiang R, Wang W and Wang H 2025 *Transp. Res. Part C Emerg. Technol.* **172** 105024
[11] Liang J H, Li Y J, Yin G D, Xu L W, Lu Y B, Feng J W, Shen T and Cai G S 2023 *IEEE Trans. Veh. Technol.* **72** 1559
[12] Liu H Q, Zheng S T, Jiang R, Tian J F, Yan R D, Zhang F and Zhang D Z 2023 *IEEE Trans. Intell. Transp. Syst.* **24** 11733
[13] Jing S C, Hui F, Zhao X M, Rios-Torres J and Khattak A J 2022 *IEEE Trans. Intell. Transp. Syst.* **23** 24248
[14] Ma K, Wang H, Zuo Z W, Hou Y X, Li X P and Jiang R 2022 *Transp. Res. Part C Emerg. Technol.* **145** 103927
[15] Brunner J S, Makridis M A and Kouvelas A 2022 *IEEE Trans. Intell. Transp. Syst.* **23** 19299
[16] Xu Y W, Chu L, Zhao D and Chang C 2021 *Machines* **9** 263
[17] Ruan T C, Wang H, Jiang R, Li X P, Xie N, Xie X J, Hao R R and Dong C Y 2024 *IEEE Trans. Intell. Transp. Syst.* **25** 462
[18] Wang W S, Liang J, Pan C F, Cai Y F and Chen L 2022 *IEEE Trans. Intell. Transp. Syst.* **23** 21062
[19] Wang Z H, Ramezani M and Levinson D 2024 *Transp. Res. Part B Method.* **186** 102994
[20] Atagoziev M, Schmidt E G and Schmidt K W 2023 *Transp. Res. Part C Emerg. Technol.* **147** 103985
[21] Shang Y, Zhu F, Jiang R, Li X G and Wang S P 2024 *Transp. Res. Part C Emerg. Technol.* **158** 104441
[22] Zheng Y, Ran B, Qu X, Zhang J and Lin Y 2020 *IEEE Trans. Intell. Transp. Syst.* **21** 4605
[23] Cheng R J, Ji Q, Zheng Y C and Ge H X 2023 *Physica A* **632** 129333
[24] Wu D M, Li Z, Du C Q, Liu C S, Li Y and Xu X 2024 *IEEE Open J. Intell. Transp. Syst.* **5** 810
[25] Heshami S and Kattan L 2024 *Transp. Res. Part C Emerg. Technol.* **166** 104789
[26] Wu G H, Wu J M, Zheng S T and Jiang R 2024 *Physica A* **652** 130044
[27] Guo N, Jiang F H, Zhu K, Wu C Y and Hao Q Y 2023 *Transp. Res. Part B Method.* **186** 102994
[28] Liu Y Y and Peeta S 2025 *Transportmetrica B: Transport Dynamics* **11** 1218
[29] Fu M H, Li S W, Guo M Z, Yang Z F, Sun Y X, Qiu C X, Wang X and Li X 2023 *Transp. Res. Part C Emerg. Technol.* **157** 104415
[30] Ma H Z, Qian C, Li L H, Qu X and Ran B 2024 *Transp. Res. Part C Emerg. Technol.* **165** 104701
[31] Xin Q, Fu R, Ukkusuri S V, Yu S W and Jiang R 2021 *Physica A* **563** 125452
[32] Chen J M, Zhou Y and Chung E D 2024 *IEEE Trans. Intell. Transp. Syst.* **25** 1897
[33] Liu H Q and Jiang R 2021 *Physica A* **575** 126055
[34] Wang S H, Zhao M, Sun D H and Wang L P 2025 *IEEE Trans. Intell. Transp. Syst.* **26** 5872
[35] Xue Y J, Zhang X K, Cui Z Y, Yu B and Gao K 2023 *Transp. Res. Part C Emerg. Technol.* **150** 104083
[36] Liu H B, Song X H, Liu B, Liu J, Gao H and Liang Y Y 2023 *Sensors* **23** 559
[37] Tajalli M, Niroumand R and Hajbabaie A 2022 *Transp. Res. Part C Emerg. Technol.* **143** 103761
[38] Dong C Y, Wang H, Li Y, Shi X M, Ni D H and Wang W 2021 *Transportmetrica A: Transp. Sci.* **17** 124
[39] Wang C, Xie Y C, Huang H L and Liu P 2021 *Accid. Anal. Prev.* **157** 106157
[40] Li X P, Cui J X, An S and Parsafard M 2014 *Transp. Res. Part B Method.* **70** 319